NANO LETTERS

Letter

pubs.acs.org/NanoLett

A Highly Elastic, Capacitive Strain Gauge Based on Percolating Nanotube Networks

Daniel J. Cohen,*[,†] Debkishore Mitra,[†] Kevin Peterson,[‡] and Michel M. Maharbiz[‡]

[†]Departments of Bioengineering and [‡]Electrical Engineering and Computer Science, University of California, Berkeley, California 94720, United States

Supporting Information

ABSTRACT: We present a highly elastic strain gauge based on capacitive sensing of parallel, carbon nanotube-based percolation electrodes separated by a dielectric elastomer. The fabrication, relying on vacuum filtration of single-walled carbon nanotubes and hydrophobic patterning of silicone, is both rapid and inexpensive. We demonstrate reliable, linear performance over thousands of cycles at up to 100% strain with less than 3% variability and the highest reported gauge factor for a device of this class (0.99). We further demonstrate use of this sensor in a robotics context to transduce joint angles.

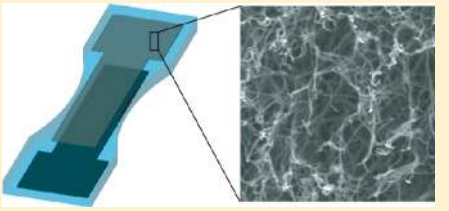

KEYWORDS: *Nanotubes, percolation, sensor, strain, elastomer*

Conventional, metal-foil strain gauges are limited to applications involving both relatively stiff substrates and strains under 5% (above which the gauge mechanically fails).[1,2] As such, they are particularly ill-suited for use in the low-stiffness, high-strain environments that characterize many medical applications and, increasingly, soft robotics systems.[3−8] Recently, many efforts to address this problem have focused on carbon nanotube-based percolation networks that are variously coupled to elastomeric matrices.[9−14] Percolating networks consist of a collection of conductive particles in two- or three-dimensions that overlap with each other to create a conductive network. Such a network is able to maintain conductivity even when deformed due to continual contact among the conductive particles. The critical concentration, or percolation threshold, required to achieve stable percolation is a direct function of the geometry of these particles and scales with aspect ratio.[15] Carbon nanotubes are particularly well suited for use in percolation networks as they have both a high intrinsic conductivity and aspect ratios as high as 1:1000.

The most common approach to percolation sensors relies on piezoresistance (strain induces a change in the resistance of the network). A variety of techniques have been developed for producing these networks using carbon nanotubes. Some of the earliest approaches relied on carefully dispersing nanotubes in unpolymerized polymer before curing the ensemble to produce a conductive composite.[7,16] While quite effective for flexible electronics, this approach results in significant reinforcement of the elastic modulus, thereby making the material to stiff for stretchable applications.[16] More recent techniques involve infiltration of an elastomer into a vertically aligned array of nanotubes grown on a wafer, direct contact transfer of wafer-grown or vacuum filtered nanotubes microcontact stamping, airbrushing of dispersed nanotubes onto a substrate, and manual assembly of sheets of aligned nanotubes onto the surface of an elastomeric support.[2,17−20] While effective, piezoresistive designs can be difficult to tune as they inherently rely on the mechanical stability of the percolation network and are susceptible to hysteresis and variable gauge factors (the normalized change in resistance divided by the applied strain) as the network adjusts over time.

An alternative approach relies on the piezocapacitance of dielectric elastomers sandwiched by percolation electrodes. Here, any deformation that brings the electrodes closer together results in an increase in capacitance, and vice versa. While these devices are most often used as low-strain pressure sensors that transduce forces normal to the sensor surface, they can also be used to transduce planar, tensile strains (Figure 1a).[8] To date, such planar strain piezocapacitors have been used to transduce strains up to 30% by using either nanotubes or conductive polymers.[20−22] While we also opted to use nanotube percolation electrodes, our design was optimized for cyclic, planar strains up to 100% (Figure 1b-c).

The general mechanism by which such a device couples planar strain to a change in capacitance relies on Poisson contraction. Uniaxial, planar strain results in a Poisson's ratio-mediated contraction of the orthogonal axes that brings the two electrodes closer together resulting in a corresponding increase in capacitance. The simplified, linear mechanics of this process (Figure 1a) are described by eqs 1−3

$$\frac{\Delta L}{L} = \varepsilon_z = \frac{\sigma_z}{E_{\text{silicone}}} \quad (1)$$

$$\varepsilon_x = \varepsilon_y = \nu\varepsilon_z \quad (2)$$

Received: November 16, 2011
Revised: March 8, 2012

   dx.doi.org/10.1021/nl204052z | *Nano Lett.* XXXX, XXX, XXX−XXX

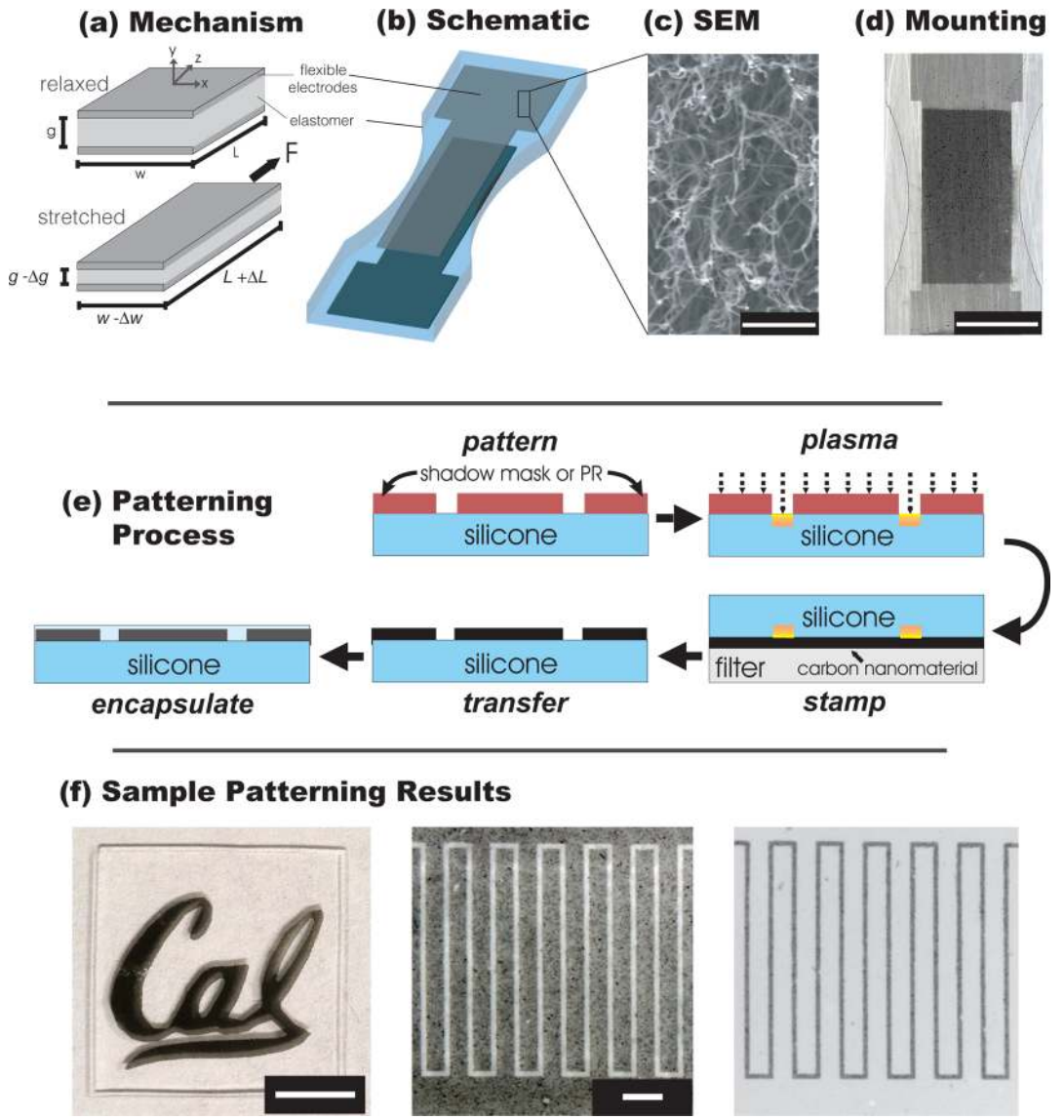

Figure 1. Mechanism, design, and fabrication of a Poisson Capacitor. (a) Poisson contraction converts planar strain to a decrease in the gap distance between the percolating electrodes and an increase in capacitance. (b) Schematic of our device geometry; all sensing is carried out in the middle region of the sensor. (c) SEM data demonstrating percolation of the nanotubes within the electrode; scale bar is 500 nm. (d) Close-up image of the sensing region of the device. Darker region is due to overlap of electrodes, and striations are due to texture of the background; scale bar is 0.75 cm. (e) Process flow for preparing a sensor. (f) Results from patterning. (left) Produced using atmospheric plasma and paper shadow-mask, fringing due to shadows; scale bar is 5 mm. (center) RIE oxygen plasma and photoresist was used to produce 300 μm wide digits; scale bar is 750 μm. (right) Nanotubes left on the filter after previous transfer, line width is 100 μm; same scale as at left.

$$L_{\text{stretch}} = L + \Delta L = L + \varepsilon_z L$$
$$w_{\text{stretch}} = w - \Delta w = w - \nu\varepsilon_z w$$
$$g_{\text{stretch}} = g - \Delta g = g - \nu\varepsilon_z g \quad (3)$$

Here, ν is Poisson's ratio (~0.5 for silicone elastomers); ε is strain; σ is stress; E is the elastic modulus of silicones; and L, w, and g are the initial dimensions of the capacitor. Equation 1 is Hooke's law relating modulus, stress, and strain. While models taken from nonlinear elasticity theory are generally used for large deformations, the simple linear model described here has an equivalent goodness-of-fit (R^2 = 0.997) to nonlinear models when fitted to mechanical testing data taken from our sample devices (Figure S1 and Supporting Information).[23]

Equations 2 and 3 describe how Poisson's ratio couples strain applied in one axis to opposite strains induced in the other two axes. If we relate this to the simplest model for parallel plate capacitance, we arrive at eq 4

$$\Delta C_{\text{simple}} = e_0 e_{\text{silicone}}\left(\frac{w_{\text{stretch}} L_{\text{stretch}}}{g_{\text{stretch}}}\right)$$
$$= e_0 e_{\text{silicone}}\left(\frac{w(1-\upsilon\varepsilon_z)L(1+\upsilon\varepsilon_z)}{g(1-\upsilon\varepsilon_z)}\right)$$
$$= e_0 e_{\text{silicone}}(1+\varepsilon_z)\frac{wL}{g} \quad (4)$$

Here, e_0 is the permittivity of free space, and e_{silicone} is the relative permittivity of silicone. This simple electromechanical equation directly relates the change in capacitance of the parallel plate geometry to the applied strain and the initial

dx.doi.org/10.1021/nl204052z | Nano Lett. XXXX, XXX, XXX–XXX

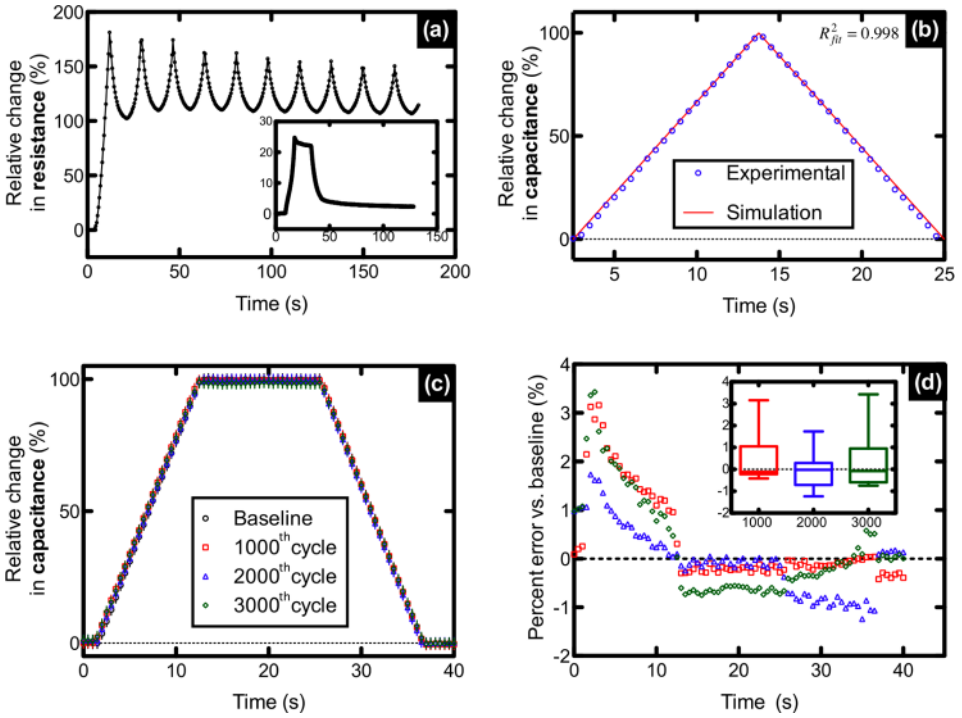

Figure 2. Performance characterization of Poisson capacitor strain gauge. (a) Resistive performance of a single percolation electrode when undergoing 100% cyclic strain. Main plot indicates significant hysteresis, while inset shows both relaxation during a 100% step strain and subsequent hysteresis during recovery. (b) Single, 100% strain cycle of the capacitive sensor (blue) overlaid (red) by the fit from parallel plate model with Palmer correction (red). (c) Demonstration of repeatability over 3000 cycles of 100% strain. After every 1000 cycles, the sample was subjected to a 100% step strain before being relaxed back to basal strain. (d) Stability plot showing how much sensor performance deviated from baseline performance over 3000 cycles. Legend is the same as for (c).

geometry of the sensor. It is interesting to note that the final equation, despite resulting from Poisson contraction, does not depend on the value of Poisson's ratio as long as the material is assumed to be isotropic. The equation further predicts a linear output, assuming that the overlap geometry remains stable. This implies that, regardless of resistive hysteresis (i.e., piezoresistive effects, changes in the percolation network nanostructure), the sensor performance remains stable as long as the effective overlap area between percolation electrodes remains stable. While this model describes the general mechanics and agrees with that used by Loh et al. to describe a strain gauge based on a stiff polymer layer with nanotube/gold particle electrodes strained at 1%, it does not take into account the fringing fields normally obtained with finite-size parallel plate capacitors. To take these into account, we used the Palmer correction factor, which is a multiplier that acts on all terms in the simple model, for all of simulations (eq S1 and Supporting Information).[24]

Our design, shown in mounted form in Figure 1d, relies on producing carbon nanotube percolation electrodes that are stable over large deformations and can be precisely patterned onto the elastomeric substrate such their shape and orientation can be specified independently of those of the elastomer. We chose silicone as the substrate both due its excellent elastomeric properties and its ability to facilitate patterning on both sides of a sheet via the hydrophobic to hydrophilic transition that results from atmospheric (or oxygen) plasma treatment.[25] As raw single-walled carbon nanotubes (SWNT) are highly hydrophobic, they will preferentially adhere to the hydrophobic (untreated) regions of the patterned silicone (Figure 1f).

Our fabrication process is summarized in Figure 1e. First, 275 μm thick silicone substrates were laser-cut into the test structures (Figure 1b). The pattern resolution necessary for the sensor electrodes was achievable using laser-cut sticker-paper masks that were applied to both sides of the silicone substrates. The masked substrate was positioned on its side in an atmospheric plasma cleaner to allow the plasma access to both sides of the silicone to render the unmasked regions hydrophilic. Upon removal from the chamber, the masks were removed and the substrate was ready to receive nanotubes. The percolation networks were produced using SWNT that were dispersed in a surfactant solution via sonication and subsequently vacuum filtered and collected on a 20 nm pore-size filtration membrane.[26,27] The result of this process is a percolation network resting on top of a filtration membrane. By bringing both sides of the plasma-treated silicone into contact with these percolation networks, we achieved direct nanotube transfer to the untreated regions of the silicone and produced the overlapping electrodes necessary for a parallel plate capacitor. Should submillimeter features be required, the shadow mask can be replaced with a photoresist layer that can be removed via acetone immersion after plasma treatment. Between these two masking techniques, we have successfully demonstrated patterns ranging from centimeters in size to 100 μm wide serpentines (Figure 1f).

As a final step to protect and stabilize the newly transferred nanotube layers, we used an airbrush to coat the substrates with thin layers of silicone while avoiding spraying the ends of the device (the contact pads).[28] All of our tested sensors were designed with a 1.7 cm × 0.75 cm electrode overlap area and an initial silicone spacer thickness of 275 μm. During testing, the

dx.doi.org/10.1021/nl204052z | Nano Lett. XXXX, XXX, XXX–XXX

contact pads were clamped against copper foil leads connected to an electrical impedance spectroscopy system (EIS). While we used EIS to precisely characterize the device performance, a capacitive Wheatstone bridge can be used as a lightweight, portable alternative. Once connected to the EIS, the sensor was placed in a customized mechanical stretcher capable of cyclically stretching the sensor to 100% strain at 2 mm/s. The fabrication process with special attention to the patterning method is discussed in greater detail in Supporting Information.

Sensors made in this fashion were cycled between 0 and 100% strain (Figure 2a). For comparison, we first tested the piezoresistive performance of our electrodes. As anticipated, there was significant resistive hysteresis that resulted in a permanent increase in baseline resistance of slightly over 100% relative to the initial resistance (~15 kΩ by two-point measurement). In addition to hysteresis, there was pronounced viscoelastic behavior (inset, Figure 2a), where the sample was strained to 100% and held at that strain for 10 s before being relaxed. During this process, it is clear that the percolation network undergoes stress relaxation. Lastly, there was a continual decrease in the piezoresistive gauge factor with cycling (~0.5 over the first 10 cycles to ~0.25).

By contrast, when used as capacitive strain sensors the performance was markedly stable and reliable. The Poisson capacitors averaged a baseline capacitance of 16 pF (n = 6; measured by EIS). All measurements used an AC excitation frequency of 10 kHz (selected by examining the frequency response curve, Supporting Information Figure S2). Devices subjected to 100% cyclic strain (Figure 2b) exhibited a relative change in capacitance (blue circles) that closely matched (R^2 = 0.998) that predicted by the linear elastic model with the Palmer correction factor (see Supporting Information). This stable performance occurs despite the wide variability in the resistive properties of the two percolation electrodes. Moreover, the performance under increasing tension versus that under decreasing tension is essentially symmetric. When comparing strain versus normalized change in capacitance for these two cases, the average slopes differed by <2%.

The actual stability of the device was assessed over the course of 3000 cycles at 100% cyclic strain (Figure 2c). During testing, a new sensor was mounted and immediately subjected to a "step-and-hold" test where it was stretched at 2 mm/s up to 100% strain and held for ~12.5 s before reversing the direction of the stretcher. This data set was taken to be the baseline response curve. Following this, the sensor was cycled from 0 to 100% strain with a sawtooth wave profile. Every 1000 cycles (up to 3000 total cycles), the sensor was subjected to an additional step-and-hold test to assess its stability. When used as a Poisson capacitor, the device exhibited stable performance with little hysteresis (Figure 2d). The offset error did not exceed 3% of the baseline, and the trend was not monotonic, implying a relatively stable network absent of significant hysteresis. To our knowledge, variability of within 3% at over 3000 cycles represents some of the lowest values reported for stretchable strain gauges (a typical value for a recent nanotube resistive strain gauge was over 10% hysteresis after the first cycle).[15] Moreover, if the data are normalized with respect to the data taken at 1000 cycles as opposed to the first cycle this error drops to less than 1.5% (data not shown), implying that there is slight settling that occurs over the first 1000 cycles.

The sensitivity of the Poisson capacitor lies very near to the theoretical limit for an elastomeric parallel plate capacitor, which predicts a gauge factor of 1. Here, the gauge factor is defined as $(\Delta C/C_o)/\varepsilon$. Calculating the mean gauge factor from the data in Figure 2c, we obtain a gauge factor of 0.99 that is uniform throughout the entire 100% strain range. A similar piezocapacitor recently reported was tested to 30% strain with a gauge factor of 0.4.[20] The only sensor to our knowledge that explored similar strain (100+%) and cyclic testing relies on a nanotube piezoresistor and has a gauge factor of 0.86 for strains less than 40%, and 0.06 for strains greater than 60%.[2] Additionally, strain gauge sensitivity can vary with temperature, and we controlled for thermally induced expansion and dielectric constant variation by conducting all experiments at 25 °C. However, we also directly calculated the sensor's sensitivity to temperature by using published values for silicone material properties and adding both thermal expansion and thermally induced dielectric constant variation into the Palmer model.[29] These calculations suggest that the sensor's capacitive output will vary on the order of 0.01 pF/°C. Given that the sensor operates on the order of 10 pF, this represents a sensitivity of 0.1%/°C, meaning that it should be fairly resistant to temperature variations.

As a demonstration of an alternative to traditional rigid transducers and encoders for robotics, we built a proof-of-concept for robotics applications where size, weight, and power strongly constrain design options. Two such examples where these constraints are crucial are the MEDIC and RoACH (platforms of centimeter-scale walking and running robots). Here, the exoskeleton of the robot consists entirely of origami-style composite laminates that have been cut and folded to produce from four to six "legs" in the form of four-bar linkages.[30−32] This process results in a strong and light robot (RoACH is only 2.4 g) but also places a premium on sensing and actuation components. At present, the legs are controlled via open-loop, contractile shape memory alloy actuators and passive return springs. Using a Poisson capacitor instead of a return spring would additionally allow feedback control, in turn allowing much more consistent locomotion and more complex behaviors.

Using the same smart composite manufacturing process as used with MEDIC and DASH, we built a scaled up version off of leg linkage and attached the Poisson capacitor in the place of the return spring. Supporting Information video S1 presents the full range of motion of the linkage when coupled to the sensor and stretching apparatus. Figure 3 presents stills of this motion sequence above a plot mapping "limb angle" to relative change in capacitance. To do this, the system was cycled through 80% strain of the sensor (limited by the geometry of the linkage), during which time the 4-bar linkage rotates the "limb" through a wide arc while the sensor stretches. In essence, this allows us to transduce changes in joint angles without relying on an angle encoder or any other traditional, rigid sensing component such as an linear variable differential transformer. While a simple demonstration, this type of sensing can clearly be scaled to a variety of different joints and linkages in a diverse array of robotics platforms.

We have demonstrated a high-strain elastomeric, parallel-plate capacitive strain gauge that relies on the Poisson effect to translate uniaxial strain into a scaled deformation that brings the two percolating electrodes closer together. By operating in this fashion, we bypass a number of the typical problems underlying percolating nanotube electrodes and piezoresistive designs such as hysteresis and a variable gauge factor. The device was fabricated using a novel hydrophobicity patterning technique that can be performed rapidly (<20 min for full

dx.doi.org/10.1021/nl204052z | Nano Lett. XXXX, XXX, XXX−XXX

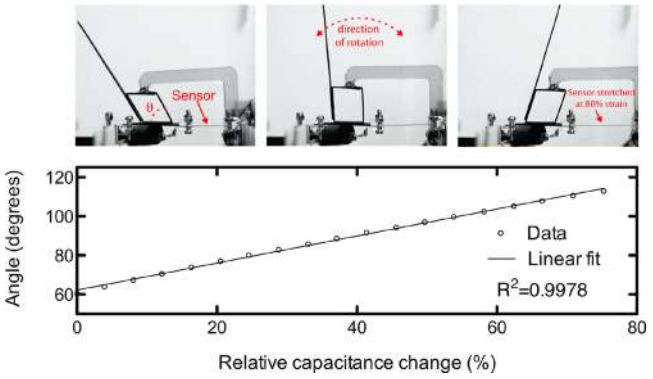

Figure 3. Demonstration of sensor as angle transducer for four-bar linkage. The image sequence is a time-lapse of the motion of a four-bar linkage limb. The sensor, attached to the base of the linkage, stretches in proportion to the amount by which the limb rotates. The plot shows the mapping between sensor output and angle of the limb. The "L"-shaped structure physically pulls on the mobile part of the four-bar linkage. See Supporting Information video S1 for the full range of motion.

assembly) with minimal equipment and at low cost (<$1/ sensor) making it an attractive option for anyone needing to rapidly prototype this type of sensor (or similar nanotube devices). Despite the anticipated, unstable resistive properties of our stretchable electrodes, the capacitive output of the sensor remains stable to within 3% over 3000 cycles. Further, the sensor exhibits the highest reported gauge factor (GF = 0.99) of any strain gauge capable of reversibly undergoing 100% strains or higher. Coupling this to the linear performance throughout the entire 100% strain cycle means that is readily calibrated and adaptable to practical sensing applications, as we have demonstrated by incorporating it into a typical robotic linkage as an alternative to an angle encoder.

■ ASSOCIATED CONTENT

Supporting Information

Characterization of the silicone mechanical properties, detailed description of the fabrication processes, discussion of the patterning technique, a discussion of the Palmer model for parallel plate capacitors, capacitance versus frequency response of the sensor, and a video of the four-bar linkage leg going through its full range of motion. This material is available free of charge via the Internet at http://pubs.acs.org.

■ AUTHOR INFORMATION

Corresponding Author

*E-mail: daniel.cohen@berkeley.edu.

Notes

The authors declare no competing financial interest.

■ ACKNOWLEDGMENTS

We thank Cary Pint, Nikta Fakhri, Nick Kohut, and Gabriel Lavella for their support and advice. Thanks also to Patrick Goodwill and Paul Lum for assistance with equipment. Funding for this project came from the National Defense Science and Engineering graduate fellowship (NDSEG) and the National Science Foundation.

■ REFERENCES

(1) Ajovalasit, a; Zuccarello, B. *J. Strain Anal. Eng. Des.* **2005**, *40*, 643−653.
(2) Yamada, T.; Hayamizu, Y.; Yamamoto, Y.; Yomogida, Y.; Izadi-najafabadi, A.; Futaba, D. N.; Hata, K. *Nat. Nanotechnol.* **2011**, 1−6.
(3) Cutkosky, M. R.; Kim, S. *Philos. Trans. R. Soc., Ser. A* **2009**, *367*, 1799−813.
(4) Rogers, J. a; Someya, T.; Huang, Y. *Science (New York, N.Y.)* **2010**, *327*, 1603−7.
(5) Lacour, S. P.; Benmerah, S.; Tarte, E.; Fitzgerald, J.; Serra, J.; McMahon, S.; Fawcett, J.; Graudejus, O.; Yu, Z.; Morrison, B. *Med. Biol. Eng. Comput.* **2010**, 945−954.
(6) Carta, R.; Jourand, P.; Hermans, B.; Thoné, J.; Brosteaux, D.; Vervust, T.; Bossuyt, F.; Axisa, F.; Vanfleteren, J.; Puers, R. *Sens. Actuators A* **2009**, *156*, 79−87.
(7) Sekitani, T.; Nakajima, H.; Maeda, H.; Fukushima, T.; Aida, T.; Hata, K.; Someya, T. *Nat. Mater.* **2009**, *8*, 494−9.
(8) Takei, K.; Takahashi, T.; Ho, J. C.; Ko, H.; Gillies, A. G.; Leu, P. W.; Fearing, R. S.; Javey, A. *Nat. Mater.* **2010**, *9*, 1−6.
(9) Sekitani, T.; Noguchi, Y.; Hata, K.; Fukushima, T.; Aida, T.; Someya, T. *Science (New York, N.Y.)* **2008**, *321*, 1468−72.
(10) Hu, L.; Yuan, W.; Brochu, P.; Gruner, G.; Pei, Q. *Appl. Phys. Lett.* **2009**, *94*, 161108.
(11) Huang, Y. Y.; Terentjev, E. M. *Adv. Funct. Mater.* **2010**, *20*, 4062−4068.
(12) Jung, Y. J.; Kar, S.; Talapatra, S.; Soldano, C.; Viswanathan, G.; Li, X.; Yao, Z.; Ou, F. S.; Avadhanula, A.; Vajtai, R.; Curran, S.; Nalamasu, O.; Ajayan, P. M. *Nano Lett.* **2006**, *6*, 413−8.
(13) Bokobza, L. *Polymer* **2007**, *48*, 4907−4920.
(14) Gui, X.; Cao, A.; Wei, J.; Li, H.; Jia, Y.; Li, Z.; Fan, L.; Wang, K.; Zhu, H.; Wu, D. *ACS Nano* **2010**, *4*, 2320−2326.
(15) Kyrylyuk, A. V.; Hermant, M. C.; Schilling, T.; Klumperman, B.; Koning, C. E.; van der Schoot, P. *Nat. Nanotechnol.* **2011**, DOI: 10.1038/NNANO.2011.40.
(16) Sekitani, T.; Noguchi, Y.; Hata, K.; Fukushima, T.; Aida, T.; Someya, T. *Science (New York, N.Y.)* **2008**, *321*, 1468−72.
(17) Shin, M. K.; Oh, J.; Lima, M.; Kozlov, M. E.; Kim, S. J.; Baughman, R. H. *Adv. Mater.* **2010**, *22*, 2663−2667.
(18) Zhou, Y.; Hu, L.; Grüner, G. *Appl. Phys. Lett.* **2006**, 22−24.
(19) Lee, K.; Lee, S. S.; Lee, J. a; Lee, K.-C.; Ji, S. *Appl. Phys. Lett.* **2010**, *96*, 013511.
(20) Lipomi, D. J.; Vosgueritchian, M.; Tee, B. C.-K.; Hellstrom, S. L.; Lee, J. a; Fox, C. H.; Bao, Z. *Nat. Nanotechnol.* **2011**, 1−6.
(21) Loh, K. J.; Kim, J.; Lynch, J. P.; Kam, N. W. S.; Kotov, N. a *Smart Mater. Struct.* **2007**, *16*, 429−438.
(22) Kollosche, M.; Stoyanov, H.; Laflamme, S.; Kofod, G. *J. Mater. Chem.* **2011**, *21*, 8292.
(23) Shergold, O. A.; Fleck, N. A.; Radford, D. *Int. J. Impact Eng.* **2006**, *32*, 1384−1402.
(24) Palmer, H. B. *Trans. Am. Inst. Electr. Eng.* **1937**, *56*, 363−366.
(25) Tsougeni, K.; Tserepi, A.; Boulousis, G.; Constantoudis, V.; Gogolides, E. *Plasma Processes Polym.* **2007**, *4*, 398−405.
(26) Hu, L.; Hecht, D. S.; Gruner, G. *Nano Lett.* **2004**, *4*, 2513−2517.
(27) Zhang, M.; Fang, S.; Zakhidov, A. a; Lee, S. B.; Aliev, A. E.; Williams, C. D.; Atkinson, K. R.; Baughman, R. H. *Science (New York, N.Y.)* **2005**, *309*, 1215−9.
(28) Choonee, K.; Syms, R. R. a.; Ahmad, M. M.; Zou, H. *Sens. Actuators A* **2009**, *155*, 253−262.
(29) Baker, E.; Barry, A. *Ind. Eng.* **1946**, 5−8.
(30) Kohut, N. J.; Hoover, A. M.; Ma, K. Y.; Baek, S. S.; Fearing, R. S. *IEEE Int. Conf. Rob. Autom.* **2011**, DOI: 10.1109/ICRA.2011.5980360.
(31) Hoover, A. M.; Fearing, R. S. *2008 IEEE Int. Conf. Rob. Autom.* **2008**, 886−892.
(32) Hoover, A. M.; Steltz, E.; Fearing, R. S. *Intelligent Robots and Systems* **2008**, 26−33, DOI: 10.1109/IROS.2008.4651149.